Optics and Spectroscopy, Vol. 99, No. 2, 2005, pp. 233–244. Translated from Optika i Spektroskopiya, Vol. 99, No. 2, 2005, pp. 248–260.

QUANTUM COMPUTERS: QUBITS AND QUGATES

A Quantum Computer Based on NV Centers in Diamond: Optically Detected Nutations of Single Electron and Nuclear Spins

A. P. Nizovtsev*, S. Ya. Kilin*, F. Jelezko, T. Gaebal**, I. Popa**, A. Gruber**, and J. Wrachtrup****

** Stepanov Institute of Physics, National Academy of Sciences of Belarus, Minsk, 220072 Belarus*

*** 3rd Institute of Physics, University of Stuttgart, Stuttgart, D-70569 Germany*

e-mail: apniz@dragon.bas-net.by

Received October 19, 2004

Abstract—In an effort to realize a two-bit processor for a quantum computer on the basis of single nitrogen–vacancy defect centers (NV centers) in diamond, the optically detected nutations of the electron spin of a single NV center in the ground state and of the nuclear spin of a ^{13}C atom located at a diamond lattice site nearest to the NV center are studied. The photodynamics of NV and NV + ^{13}C centers under different temperatures and optical excitation conditions is discussed. A seven-level model of a center excited by radiation from an Ar^+ laser at room temperature is proposed. On the basis of this model, the experimental spectra of optically detected electron paramagnetic and electron–nuclear double resonances of single NV and NV + ^{13}C centers in diamond nanocrystals, as well as experimental data on the optically detected nutations of the electron and nuclear spins of these centers caused by the actions of pulsed microwave and radiofrequency fields, respectively, are interpreted. © *2005 Pleiades Publishing, Inc.*

1. INTRODUCTION

In recent years, much attention in quantum optics has been paid to the study of single nitrogen–vacancy defect centers (NV centers) in diamond. Due to their high fluorescence quantum yield and remarkable photostability, these centers proved to be promising for creation of single-photon generators [1], use as light sources in near-field spectroscopy [2], and realization of the processor of a quantum computer on the basis of the nuclear spins of ^{13}C atoms nearest to such centers [3]. A particular feature of a quantum computer based on NV centers is that it operates with pure spin states; in addition, both the optical initiation and the optical reading of the spin states of NV centers are possible [4, 5]. Recently, the optically detected nutations of a single electron spin of a single NV center [6] and the nutations of a single ^{13}C nuclear spin [7] in the system single NV center + single ^{13}C nucleus (single NV + ^{13}C center), which were caused by the action of pulsed microwave (MW) and radiofrequency (RF) fields, respectively, have been studied experimentally. These experiments became important steps on the road to realizing the idea of [3] on creation of a quantum computer based on NV centers since these experiments provided information necessary for the formation of MW and RF pulses with predetermined characteristics (e.g., π- or $\pi/2$ pulses). This made it possible to realize for the first time a CROT logic gate between two qubits, whose physical carriers were single electron and nuclear spins of the NV + ^{13}C center [7]. In addition, the authors of [6, 7] measured the rates of dephasing of the electron and nuclear spins of single NV + ^{13}C centers under the action of a fluctuating spin environment, whose values are critical for the realization of the quantum processor on the basis of NV centers. The objective of this study is to analyze in detail the new experimental data of [6, 7] on optically detected nutations of single electron and nuclear spins of NV and NV + ^{13}C centers. This theoretical analysis will be performed on the basis of a recently proposed seven-level photophysical model of an NV center [8], which is modified here as applied to the conditions of the experiments of [6, 7].

2. PHOTOPHYSICS OF THE NV CENTER

Despite the long history of study of NV centers by standard spectroscopic techniques (hole burning, four-wave mixing spectroscopy, echo spectroscopy, optically detected magnetic resonance spectroscopy, etc.) [9, 10], many aspects of the very nontrivial photophysics of NV centers remained unclear until recently. Various experiments with single NV centers performed during the last few years [4, 11–13] provided new unique information on their characteristics and made it possible to formulate a photophysical model of the NV center [8] corresponding to the experimental conditions of [4] (helium temperatures, optical excitation of the center in resonance with its zero-phonon line at $\lambda \sim 637$ nm). In [6, 7], the nutations of the electron and nuclear spins

0030-400X/05/9902-0233$26.00 © 2005 Pleiades Publishing, Inc.

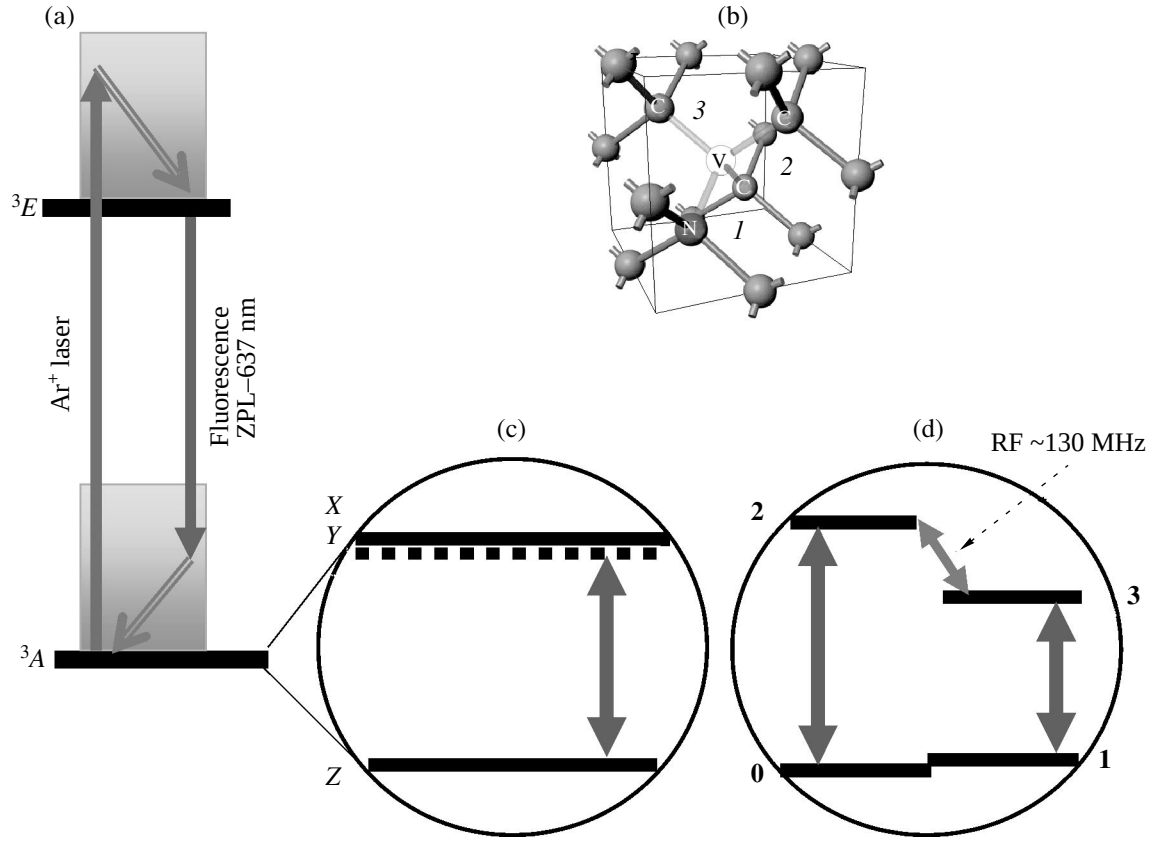

Fig. 1. (a) Schematic of (i) transitions upon optical excitation of an NV center by an Ar^+ laser, (ii) internal conversion in the vibrational band of the ^3E state, (iii) fluorescence, and (iv) internal conversion in the ^3A state. (b) Schematic of the structure of an NV center in the diamond lattice; the figures *1*, *2*, and *3* indicate carbon atoms nearest to the vacancy. (c) Fine and hyperfine structures of the ground electronic ^3A state of an NV center. (d) Fine and hyperfine structures of the ground electronic ^3A state of an NV + ^{13}C center with possible transitions induced by MW (~2.88 GHz) and RF (~130 MHz) fields.

of single NV and NV + ^{13}C centers caused by the action of MW and RF fields were observed at room temperature and under nonresonance optical excitation of single centers by an Ar^+ laser (λ = 514.5 nm). Since the photophysics of NV centers depends substantially on both the temperature and the optical excitation conditions, initially, we will discuss its particular features for various experimental conditions in the context of the photophysical model of [8].

As is known [9], an optically excited NV center emits bright red fluorescence, which has a narrow zero-phonon line (ZPL) at $\lambda \sim 637$ nm and a broad (~200 nm) phonon sideband (Fig. 1a). A distinctive feature of the center is that the optical transition occurs between the ground ^3A and excited ^3E triplet states. The diamond crystal field splits each of these states into three sublevels corresponding to the projections $m_S = \pm 1, 0$ of the triplet spin $S = 1$ of the two unpaired electrons of the NV center. In an ideal crystal and in the absence of an external magnetic field, the sublevels $m_S = \pm 1$ (the sublevels X and Y in Fig. 1c) of the ground ^3A state are degenerate and are located about 2.88 GHz above the sublevel $m_S = 0$ (the sublevel Z in Fig. 1c). The fine structure of the zero-phonon state ^3E, which is an orbital doublet, is mainly determined by spin–spin interactions [14] and depends on the strain experienced by a given center. These interactions split the ^3E state into two groups of spin sublevels: T'' ($T'' = X'', Y'', Z''$) and T' ($T' = X', Y', Z'$), which are spaced by ~40 cm^{-1} from each other. The higher T'' sublevels relax rapidly to the lower T' sublevels (the relaxation time is less than 1 ns [15, 16]), affecting insignificantly the photophysics of the center. In addition, the NV center has a metastable singlet state ^1A (Fig. 2) to which it can pass as a result of the intersystem crossing (ISC) transition $^3E \longrightarrow {}^1A$. This leads to a cessation of the fluorescence due to the ^3A–^3E transition emitted by the center upon its continuous optical excitation. The estimates show that the ^1A state is located near the ^3E state (approximately 400 cm^{-1} below the ^3E state [12]). Since spin-forbidden ISC transitions are caused by anisotropic interactions, then, as a rule, the rates of such transitions from different spin sublevels T' of the ^3E state are different. The analysis of the experiments of [4] performed in [8] within the framework of

the seven-level model of the NV center, presented in Fig. 2, showed that the rates of the ISC transitions $^3E \longrightarrow {}^1A$ from the sublevels X' and Y' (a few MHz) exceed substantially the rate of the ISC transition from the sublevel Z' (a few kHz). At the same time, the rates of the ISC transitions from the singlet ^1A state to different sublevels T of the ground triplet ^3A state proved to be considerably smaller (a few Hz) and little different from each other. As a result of this spin-selectivity of the ISC transitions, only one optical transition, namely, the transition $Z \longleftrightarrow Z'$ to the state Z', from which the center rarely passes to the singlet state, makes the main contribution to the fluorescence emitted by the center.

At low (helium) temperatures, the singlet state ^1A becomes a trap, in which the center resides for a long time since the reverse transitions from this state $^1A \longrightarrow {}^3E$ induced by phonons are practically absent and the depletion of the ^1A state occurs mainly due to infrequent ISC transitions $^1A \longrightarrow {}^3A$. As a result, the average fluorescence intensity emitted by the center proves to be low and the observation of single centers becomes difficult [12]. Only recently, the problem of the experimental observation of single NV centers at low temperatures was solved [4], which made it possible to observe the fine structure of the transition $^3A \longrightarrow {}^3E$ in the spectrum of the fluorescence excitation of single centers and to measure the correlation function $g^{(2)}(\tau)$ of the fluorescence intensity emitted by centers. Conversely, at room temperature, the ^1A state is efficiently depleted due to the reverse phonon-induced transitions $^1A \longrightarrow {}^3E$, shown in Fig. 2. As a result, this state does not affect so significantly the average fluorescence intensity of the centers, allowing one to observe them reliably [6, 7, 11, 12].

The radiation of the Ar^+ laser ($\lambda \sim 514$ nm), used in [6, 7] for the optical excitation of single NV centers, induces a vertical Franck–Condon transition to one of the highly excited vibrational levels of the ^3E state [17], which is accompanied by fast (in a matter of one femtosecond) internal conversion to the zero-phonon level, from which the center either emits a fluorescence quantum or passes to the ^1A singlet state. Since the projection of the electron spin does not change during the optical transition and in the process of internal conversion, the optical excitation from different magnetic sublevels of the ^3A state occurs according to the selection rules $\Delta m_S = 0$ [8]. In this case, the excitation probabilities of the transitions $T \longrightarrow T'$ ($T = X, Y, Z$; $T' = X', Y', Z'$) can be considered to be identical and equal to B, where B is the Einstein coefficient for the absorption. Since the excitation with the Ar^+ laser is nonresonant and the internal conversion to the zero-phonon state is fast, forced optical transitions $T' \longrightarrow T$ are absent. Spontaneous transitions $T' \longrightarrow T$ also occur according to the selection rules $\Delta m_S = 0$ and are characterized by identical rates A. All these optical transitions are indicated in Fig. 2 by vertical arrows. Another feature of the

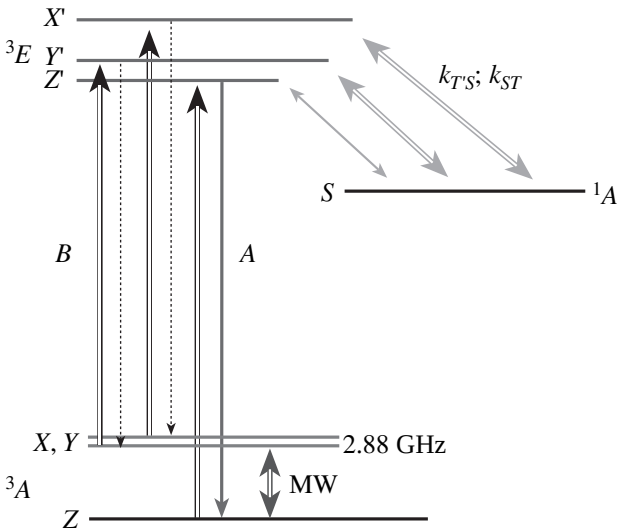

Fig. 2. Energy level diagram of a seven-level model of an NV center, which takes into account the fine structure of the ground ^3A and excited ^3E electronic states (the upper and lower spin sublevels with $m_S = 0$, +1, and –1 are denoted as Z and Z', X and X', and Y and Y', respectively). The transitions indicated by the vertical double-line arrows correspond to the excitation of the center by an Ar^+ laser according to the selection rules $\Delta m_S = 0$. In terms of the model, all these transitions have the same probability B (the Einstein coefficient for the corresponding induced absorption). The vertical single-line arrows indicate the spontaneous transitions, occurring with the same probability A. The ISC transitions $T' \longrightarrow {}^1A$ (as well as the reverse transitions $^1A \longrightarrow T'$), whose probabilities $k^0_{T'S}$ ($k^0_{ST'}$) are different, are shown by the inclined arrows of different thickness. In addition to the ISC transitions, the Ar^+ laser induces the transitions $T' \longrightarrow {}^1A$ and $^1A \longrightarrow T'$ via excited singlet states, whose probabilities are proportional to the intensity I_{opt}. As a result, the total rates of these transitions are equal to $k_{T'S} = k^0_{T'S} + k^{opt}_{T'S} I_{opt}$ and $k_{ST'} = k^0_{ST'} + k^{opt}_{ST'} I_{opt}$. There are also transitions between sublevels of the ground state induced by the environment, which are considered to occur with the same rate d. Since $k_{Z'S} \ll k_{X'S}, k_{Y'S}$, only the transition $Z' \longrightarrow Z$ makes the major contribution to the fluorescence intensity emitted by the center.

optical excitation of NV centers with the Ar^+ laser is that, in addition to the phonon-induced ISC transitions $^3E \longleftrightarrow {}^1A$, the laser irradiation produces so-called optical shelving–deshelving [12, 18] (presumably, via excited singlet states), which makes additional contributions to the rates of the transitions $^3E \longleftrightarrow {}^1A$ (which depend on the intensity of the laser radiation). At room temperature and upon optical excitation with the Ar^+ laser, the ISC transitions $^1A \longrightarrow {}^3A$, whose rate is small, can be neglected.

An important consequence of the spin-selectivity of the ISC transitions in an NV center is the optical alignment of the center, i.e., the establishment of a non-Bolt-

zmannian population distribution of the spin sublevels X, Y, and Z of the ^3A state under the action of optical excitation. It was shown in [8, 19] that, at low temperatures and upon spin-projection selective optical excitation (the excitation into the ZPL), the X and Y spin sublevels of the NV centers are predominantly populated. The spectroscopic manifestations of such an alignment are complex hole burning spectra of the inhomogeneously broadened transition ^3A–^3E, repeatedly observed previously [19]. Conversely, upon nonselective excitation by the radiation from the Ar^+ laser, the centers are predominantly aligned in the state Z [20, 21]. The populations of the spin sublevels T of the ground electronic state ^3A produced by the optical excitation can be changed by means of action on the centers with MW radiation at a frequency of ~2.88 GHz, which, in turn, should change the average fluorescence intensity emitted by the centers. The latter circumstance forms the basis for the method of optically detected electron spin resonance (OD ESR), whose sensitivity is $\sim 10^7$ times greater than that of the conventional methods of ESR spectroscopy [22]. This makes it possible to observe a wide range of OD ESR phenomena related to single spins [5]. In particular, upon optical excitation of an NV center by radiation of an Ar^+ laser and scanning of the frequency of continuous MW radiation through the Z–(X, Y) resonance, the fluorescence intensity exhibits a ~10% dip centered at ~2.88 GHz [9, 11] (the negative OD ESR effect). This minimum arises because the MW radiation decreases the population of the Z state, whose optical excitation makes the main contribution to the fluorescence. If a constant magnetic field is applied to the sample, the OD ESR line splits into two components corresponding to the nondegenerate transitions Z–X and Z–Y (Fig. 3a). If a single NV center excited by continuous laser radiation is subjected to MW pulses of variable duration T, the fluorescence intensity of the center due to its Z–X- or Z–Y spin transition exhibits nutations in relation to T (Figs. 4, 5). Previously, such nutations of the electron spin were observed for ensembles of NV centers [9]. In [6], they were observed for the first time for single NV centers.

Let one of the lattice sites nearest to the vacancy of an NV center (position 1, 2, or 3 in the first coordination sphere in Fig. 1d) be occupied by a ^{13}C carbon atom, whose nuclear spin is $I = 1/2$. We will term such a center an NV + ^{13}C center. The hyperfine interaction of this nuclear spin with the electron spin $S = 1$ of the center will result in a splitting of the nuclear spin sublevels $m_I = \pm 1/2$ by ~130 MHz [23] in the case of the states $m_S = \pm 1$. In the electron spin state $m_S = 0$, the splitting of the states $m_I = \pm 1/2$ due to the nuclear Zeeman interaction proves to be much smaller (a few MHz). Therefore, in the ground electronic state and in the absence of an external magnetic field, the NV + ^{13}C center has four spin (electronic and nuclear) states: $\mathbf{0} = |0\rangle_e|0\rangle_n$, $\mathbf{1} = |0\rangle_e|1\rangle_n$, $\mathbf{2} = |1\rangle_e|0\rangle_n$, and $\mathbf{3} = |1\rangle_e|1\rangle_n$ (Fig. 1d). Here, $|0\rangle_e = (|\uparrow\downarrow\rangle + |\downarrow\uparrow\rangle)/\sqrt{2}$, $m_S = 0$ and $|1\rangle_e = (|\uparrow\uparrow\rangle + |\downarrow\downarrow\rangle)/\sqrt{2}$, $m_S = \pm 1$ are the electronic and $|0\rangle_n = (|\uparrow\rangle$, $m_I = -1/2$ and $|1\rangle_n = (|\downarrow\rangle$, $m_I = 1/2$ are the nuclear spin states. According to the selection rules for the ESR and NMR transitions ($\Delta m_S = \pm 1$, $\Delta m_I = 0$ and $\Delta m_I = \pm 1$, $\Delta m_S = 0$, respectively), there are four allowed transitions between these spin states: **0**–**2**, **1**–**3**, **2**–**3**, and **0**–**1** (in the notation of Fig. 1d). The first two of these transitions are induced by an MW field (~2.88 GHz), while the third one is initiated by an RF field (~130 MHz). Upon continuous optical excitation of the NV + ^{13}C center and scanning of the MW field through the **0**–**2** and **1**–**3** resonances, the fluorescence spectrum exhibits a characteristic pair of OD ESR lines spaced from each other by ~130 MHz (Fig. 3b). In turn, under continuous optical excitation that is in resonance with one of the ESR transitions (**0**–**2** or **1**–**3**) and upon scanning of the frequency of the RF field through the **2**–**3** resonance, the fluorescence spectrum exhibits a line of optically detected electron–nuclear double resonance (ODENDOR), which is located at a frequency of ~130 MHz (Fig. 3c). As in the case of the ordinary NV centers, if the NV + ^{13}C center is subjected to a pulsed MW field of variable duration that is in resonance with either the **0**–**2** or the **1**–**3** transition, the dependence of the population of the sublevel Z of the center on the pulse duration T exhibits nutations, which result in corresponding nutations in the fluorescence intensity emitted by the center. Similarly, if the optically aligned NV + ^{13}C center is subjected to MW radiation that induces either the **0**–**2** or the **1**–**3** transition, the states $m_S = \pm 1$ are populated, and, in this case, the action of a pulsed RF field with a variable pulse duration T and a frequency of ~130 MHz will cause fluorescence nutations due to the **2**–**3** transition (Fig. 6). If the electronic $|0\rangle_e$ and $|1\rangle_e$ and nuclear $|0\rangle_n$ and $|1\rangle_n$ states of the system of two interacting electron and nuclear spins of a single NV + ^{13}C center are considered as qubits, then, upon corresponding choice of the parameters of MW and RF pulses, these pulses can realize different logic gates between these qubits. As was noted above, in [7], a CROT logic gate between these qubits was realized for the first time. The interactions of the single NV + ^{13}C center with the Ar^+ laser radiation and with the MW radiation do not differ from the analogous interactions of these types of radiation with the ordinary NV center, whose sublevels are split by 130 MHz in an external magnetic field. Therefore, considering, for simplicity, the **0** and **1** states as one degenerate state (**0**, **1**), the photophysics of the NV + ^{13}C center and the experiments of [7] on the observation of the optically detected nutations of the nuclear spin can be described in terms of the model of the center presented in Fig. 2.

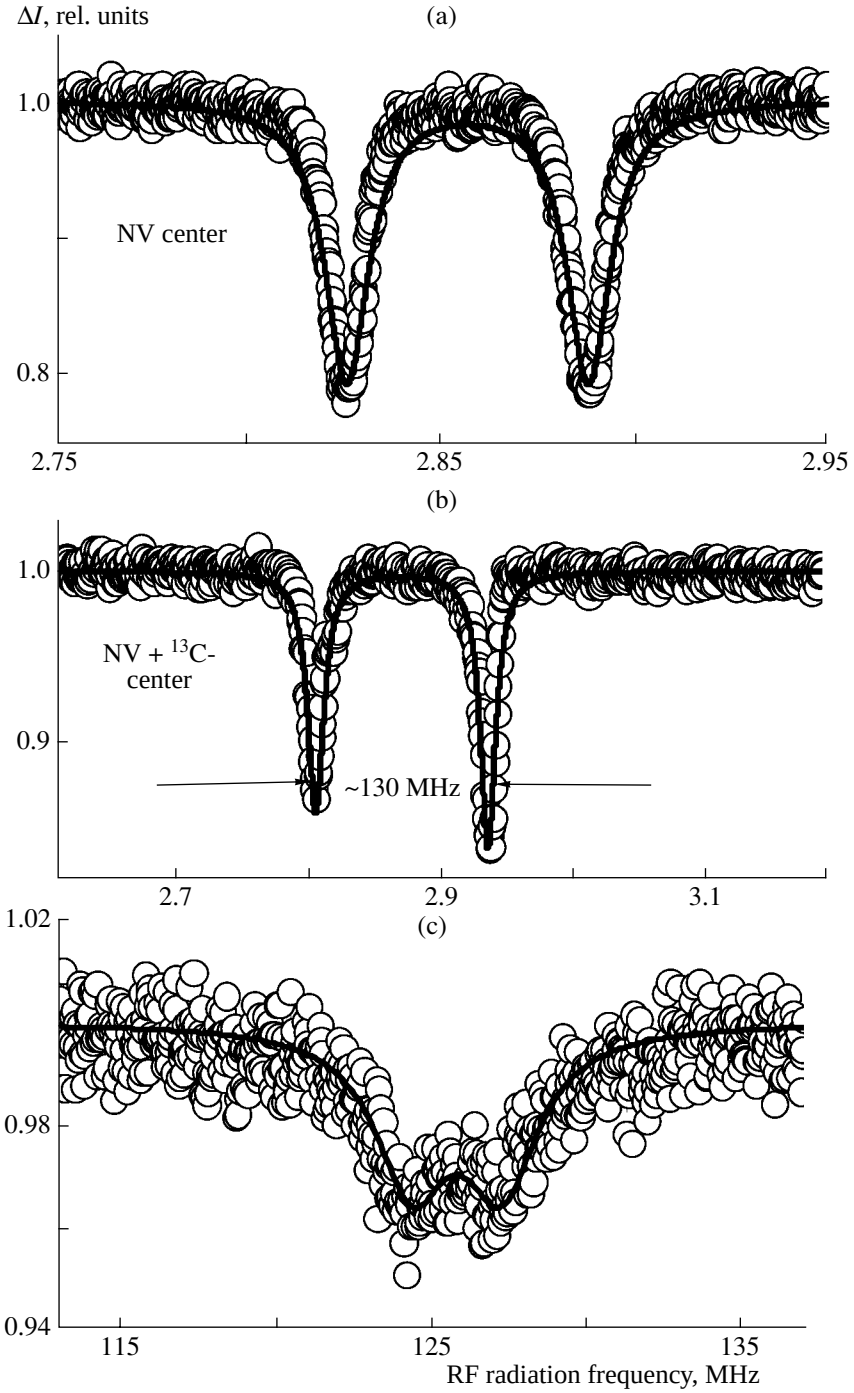

Fig. 3. Optically detected spectra of (a, b) ESR and (c) ODENDOR of single (a) NV and (b, c) NV + ^{13}C centers. The circles indicate the experimental data, and the solid lines are the theoretical fitting on the basis of the model of the center shown in Fig. 2. The following values of the parameters of the model were common to all the theoretical curves: $A = 7$ MHz [24], $b = 1.15 \times 10^{-5}$, $k^0_{X'S} = k^0_{Y'S} \sim A/2$, $k^0_{Z'S} \sim 20$ kHz, $k^0_{ST'} = k^0_{T'S}/40$, $d \sim 1$ kHz, $k^{opt}_{Z'S} = 0.143\,b$, $k^{opt}_{SZ'} = 0.417\,b$, and $K^0 \sim 300$ kHz. In addition, it was assumed that there are no optical contributions to the transition rate constants X', $Y' \longleftrightarrow S$ ($k^{opt}_{Y'S} = k^{opt}_{X'S} = k^{opt}_{SY'} = 0$). The values of the other parameters were as follows: (a) $\omega_{XY} = 62$ MHz, $V_1 = 0.5$ MHz, and $B = A/15$; (b) $\omega_{XY} = 130$ MHz, $V_1 = 1$ MHz, and $P_{opt} = 5$ μW (a slight difference between the amplitudes of the two minima was achieved by introducing of an insignificant difference between the rate constants of the ISC transitions $k^0_{X'S}$ and $k^0_{Y'S}$); and (c) $V_1 = 1.5$ MHz, $V_2 = 0.4$ MHz, and $P_{opt} = 10$ μW. The shapes of the OD ESR and ODENDOR lines virtually do not depend on the nuclear spin dephasing rate constant K_{XY}, which can be significantly smaller than the corresponding rate constant of the electron spin K^0. Here and below, ΔI is the relative change in the fluorescence intensity.

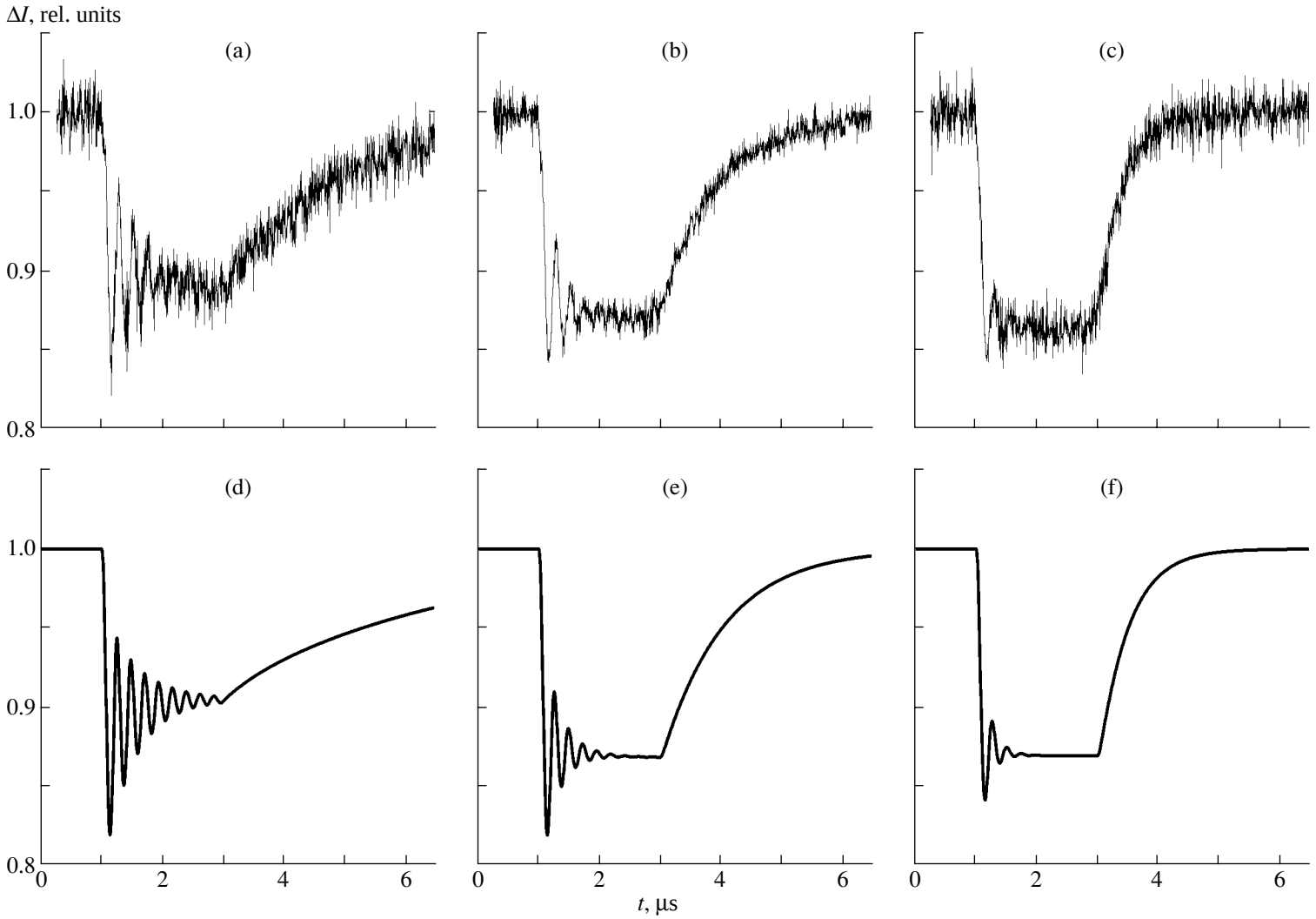

Fig. 4. (a–c) Experimentally observed and (d–f) theoretically calculated nutations of the electronic spin of an NV center under nondark experimental conditions (see the text) for three different powers of the optical radiation: P_{opt} = (a, d) 3.6; (b, e) 11; and (c, f) 22 μW. The parameters of the model are the same as those listed in the legend of Fig. 3, except that $k_{SZ'}^{opt} = 0.68\,b$, and V_1 = 2.25 MHz.

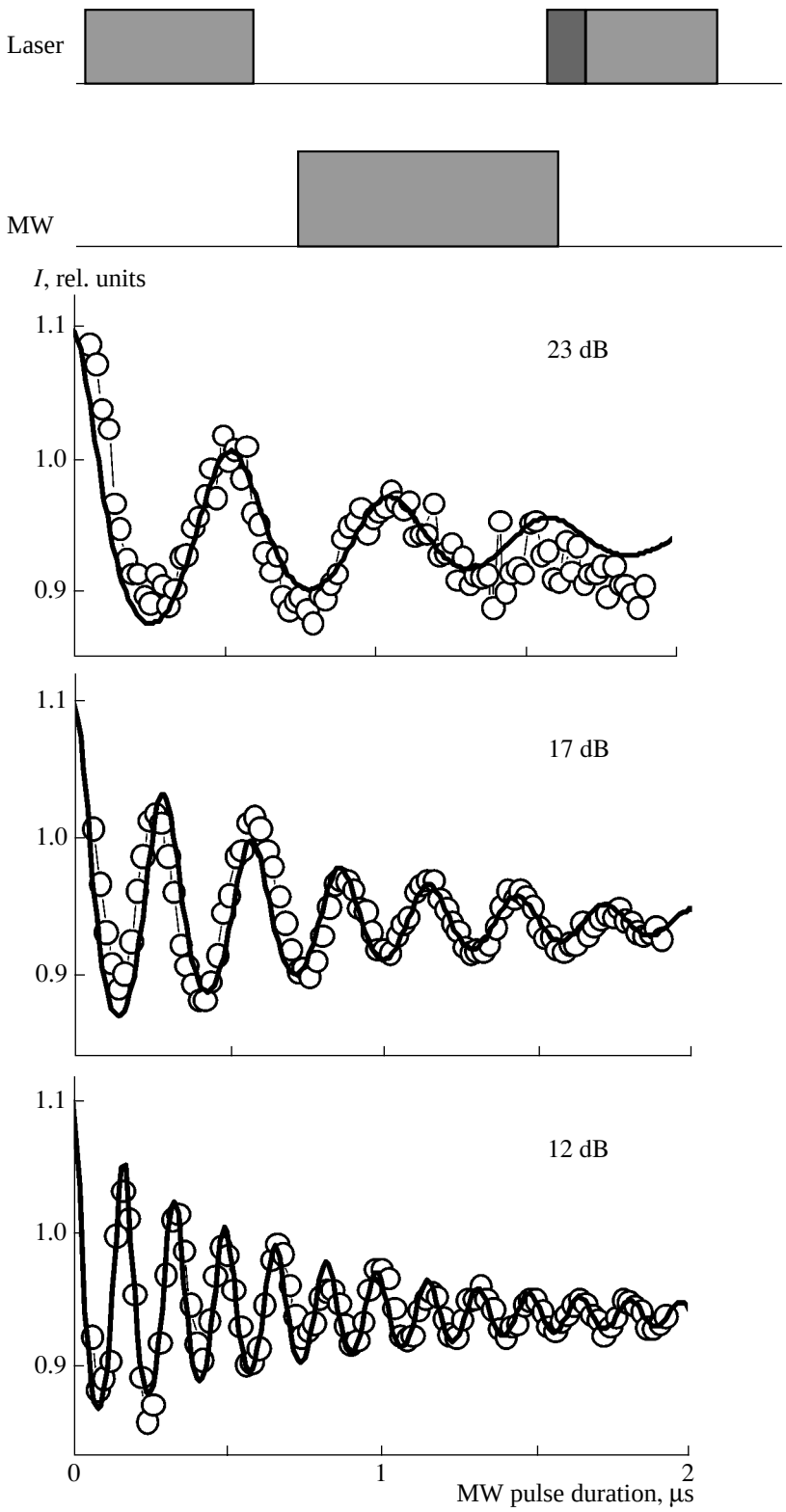

Fig. 5. Experimentally observed (circles) and theoretically calculated (solid lines) nutations of the electronic spin of an NV center under dark experimental conditions (see the text) for three different powers of the MW radiation corresponding to the standard radiation attenuation of 23, 17, and 12 dB. The parameters of the model are the same as those listed in the legend of Fig. 3. The power of the optical radiation was P_{opt} = 10 μW. The 23, 17, and 12 dB attenuations correspond to V_1 = 3.05, 1.75, and 0.95 MHz. In calculations, the signal detected was averaged over the series, which included a tenfold repetition of the sequence of the laser and MW pulses shown at the top.

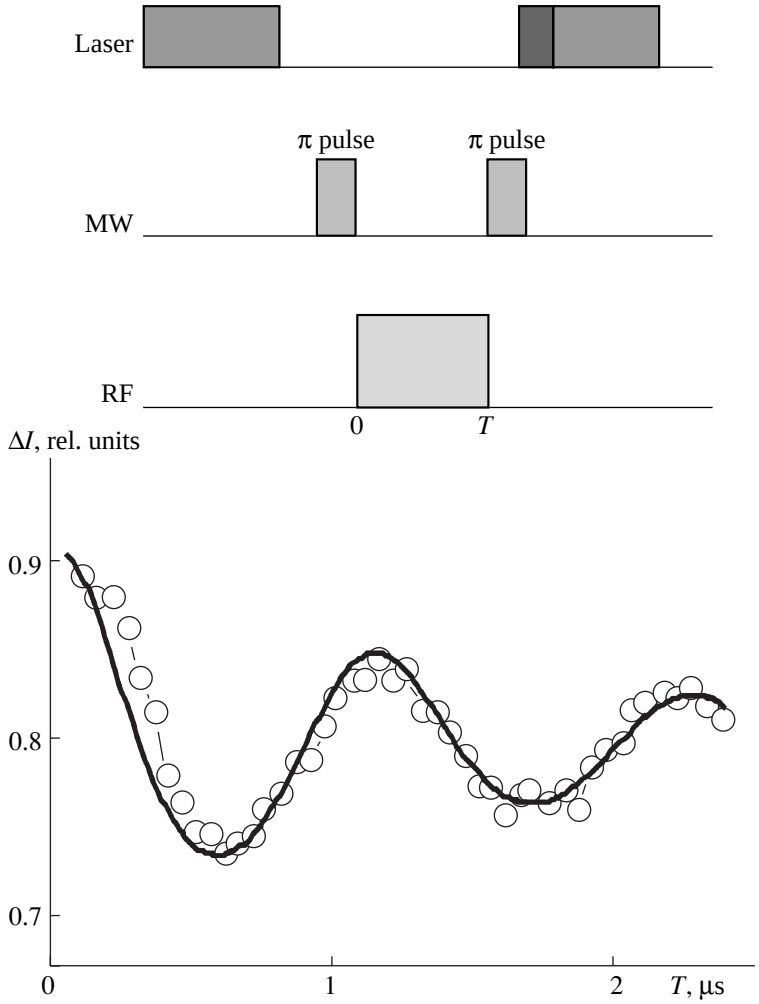

Fig. 6. Experimentally observed (circles) and theoretically calculated (solid lines) nutations of the single nuclear spin of an NV + ^{13}C center under dark experimental conditions (see the text). The parameters of the model are the same as those listed in the legend of Fig. 3. For the fitting, the following values of the parameters were taken: P_{opt} = 8.4 μW, V_2 = 0.45 MHz, $k_{SZ'}^{opt} = 0.3b$, and K_{XY} = 150 kHz. In calculations, the signal detected was averaged over the series, which included a tenfold repetition of the sequence of the laser, MW, and RF pulses shown at the top.

3. EXPERIMENT

The OD ESR and ODENDOR spectra and nutations of the electron and nuclear spins of single NV and NV + ^{13}C centers were measured at the 3rd Institute of Physics, University of Stuttgart. A confocal microscope operating at room temperature was used in these experiments. The samples were in the form of synthetic nanocrystals of type *Ib* diamond dispersed over a polymer substrate (the average size of the nanocrystals was ~20 nm). The NV centers were created by irradiation of the nanocrystals with electrons and subsequent annealing at a temperature of 900°C. For the optical excitation of the centers, we used focused radiation (with a spot diameter of ~0.5 μm) from an Ar^+ laser with the wavelength λ = 514.5 nm. Upon spatial scanning of the sample with the laser beam, nanocrystals with NV centers were detected by a characteristic fluorescence emission, whose ZPL was located at λ ~ 637 nm. The occurrence of only one center in a given nanocrystal was determined by observing the antibunching of photons emitted by the center upon measuring the correlation function $g^{(2)}(\tau)$ of the fluorescence intensity. Since diamond nanocrystals have 1.1% of naturally occurring ^{13}C isotopes, approximately every 30th nanocrystal of all the nanocrystals with identified single NV centers actually contained a single NV + ^{13}C center.

Once a diamond nanocrystal with a single NV center was spatially localized, the OD ESR spectrum of the center was measured. The circles in Fig. 3a represent a typical OD ESR spectrum of an ordinary NV center subjected to a weak constant magnetic field, which removed the degeneracy of the *X* and *Y* states and split (here, by ~62 MHz) the OD ESR line into two components. A typical OD ESR spectrum of a single NV + ^{13}C

center, having a characteristic splitting of the **2** and **3** states by ~130 MHz, is shown in Fig. 3b. Finally, the circles in Fig. 3c represent the experimental fluorescence spectrum of a single NV + ^{13}C center that was continuously excited by the Ar^+ laser radiation and by the MW radiation tuned to resonance with the **1**–**3** transition of the center and recorded upon scanning of the frequency of the RF field through the **2**–**3** resonance (~130 MHz). Actually, the spectrum in Fig. 3c is the ODENDOR spectrum of a single ^{13}C nuclear spin in an NV + ^{13}C center recorded for the first time. The splitting of the ODENDOR resonance by ~3 MHz is caused by the Autler–Townes effect, i.e., by the splitting of state **3** into two sublevels by the resonance MW radiation acting in the adjacent **1**–**3** transition.

The experiments on the observation of the electron spin nutations of an ordinary single NV center were performed with the single center whose OD ESR spectrum is shown in Fig. 3a. The frequency of the MW radiation coincided with the frequency of the *Y*–*Z* transition. The duration of the MW pulses amounted to 2 μs. The fluorescence intensity was continuously measured with a detector (during 5-ns time intervals). In the first series of experiments, the laser excitation was continuous, i.e., acted during the MW pulses. The experimental data obtained for three different powers of the laser radiation are shown in Figs. 4a–4c. In all the experiments, the intensity of the MW radiation was the same. All the measurements were averaged over ~10^5 cycles. Figures 4a–4c show that, as an MW pulse is switched on, the fluorescence intensity exhibits nutations, whose decay rate quickly increases with increasing power of the laser excitation in accordance with an increase in the dephasing rate of the electron spin in the ^3A state due to the laser-induced transitions $^3A \longrightarrow {}^3E$. As the MW pulse is switched off, the fluorescence intensity returns to its steady-state value during a time interval depending on the laser radiation intensity.

It follows from Figs. 4a–4c that the contribution of the optical transitions to the dephasing of the electron spin is determining for the given center. In order to eliminate this optical contribution to the dephasing and to measure the genuine spin dephasing rate under the action of the environment (e.g., the dephasing of the states of the single electron spin due to fluctuations of the spin environment of the center upon mutual flipping of the electron spins of the substitutional nitrogen atoms in the diamond lattice), we conducted a second series of so-called "dark" experiments. In this series, the electron spin nutations of the NV center were observed in the absence of the optical radiation during the action of the MW pulse. As in the experiments whose results are presented in Figs. 3a and 4a–4c, the sample was subjected to a weak magnetic field, while the pulsed MW radiation was in resonance with the *Z*–*Y* transition. The sequence order of laser and MW pulses used in this series of experiments is shown at the top of Fig. 5. Initially, a laser pulse with a duration of 1 μs caused the center to pass predominantly to the state *Z*; then, after the cessation of this pulse and a 0.1-μs delay, during which the excited ^3A and ^1A states were depleted for the most part, an MW pulse with a variable duration *T* was switched on, which initiated electron spin nutations. The final state of the spin after the cessation of the MW pulse was determined optically by switching on a second 1-μs laser pulse and counting the fluorescence photons emitted by the center during the first 0.3 μs. Such a sequence of laser and MW pulses was repeated ~10^5 times and the results were averaged. The circles in Fig. 5 represent the electron spin nutations of the NV center experimentally observed under dark conditions for three different intensities of the MW field. It is seen from this figure that the decay rate of the nutations is smaller as compared to the nondark case of Fig. 4 and remains approximately constant (~350 kHz), while the period of the nutations increases with increasing MW radiation intensity. The first minimum on these nutation curves corresponds to a maximal inversion of the *Z*–*Y* transition, and, in fact, its position determines the duration of the MW π pulses.

The single NV + ^{13}C centers were identified by the occurrence (in the absence of a constant magnetic field) of a characteristic ~130 MHz splitting of the OD ESR spectrum, whose typical shape is shown by the circles in Fig. 3b. The electron spin nutations of the single NV + ^{13}C centers were observed under dark conditions in the same way as in the above-described case of the ordinary NV centers. The MW radiation was tuned to resonance either with the **0**–**2** or with the **1**–**3** transition. In both cases, the nutations observed were similar to those shown in Fig. 5. These observations of the electron spin nutations made it possible to determine the parameters of the MW π pulses that were used for inverting the populations of the **0**–**2** and **1**–**3** transitions in subsequent experiments on studying the ODENDOR line due to the **2**–**3** transition of the single NV + ^{13}C center. In particular, the nutations of the single ^{13}C nuclear spin shown by the circles in Fig. 6 were observed under dark conditions using the sequence order of laser, MW, and RF pulses shown at the top of the figure. Initially, a laser pulse with a duration of 3 μs [7] transferred the NV + ^{13}C center to the state $m_S = 0$ (the **0** or **1** state); then, an MW π pulse resonant to the **1**–**3** transition inverted the populations of the **1** and **3** states. After that, an RF pulse of variable duration initiated resonance transitions between the **3** and **2** states and caused nuclear spin nutations. After the cessation of this pulse, the population of state **3** was determined with the help of a second MW π pulse, which inverted the populations of the **3** and **1** states, and a second 3-μs laser pulse, during the first 0.3 μs of which the detector measured the fluorescence photons emitted by the center. As previously, this sequence of the laser, MW, and RF pulses was repeated ~10^5 times and the results of the photon counting were averaged to yield the experimental

dependence of the fluorescence intensity on the RF pulse duration, which is shown by the circles in Fig. 6.

4. THEORY

As was noted in Section 2, to describe the OD ESR and ODENDOR spectra shown in Fig. 3, as well as the optically detected nutations of the electron and nuclear spins shown in Figs. 4–6, we used the seven-level model of the NV and NV + ^{13}C centers shown in Fig. 2. Since all the experimental data were obtained by averaging over a large number of points and because the system under study possesses the property of ergodicity, to interpret the experimental results, we used the standard Bloch equations for the density matrix ρ_{ij}^t of the model system of Fig. 2. In these equations, the optical excitation of the NV center from the zero-phonon state ^3A to the zero-phonon state ^3E was described with the help of the probability B of a transition induced by an Ar^+ laser. This probability can be written as $B = bI_{\text{opt}}$, where I_{opt} is the intensity of the optical excitation and $b = 8\pi p_{eg}^2/c\hbar^2\gamma$ is the Einstein differential coefficient, in which p_{eg} is the dipole moment of the $^3A \longrightarrow {}^3E$ electronic transition of the NV center and γ is internal conversion rate constant for the ^3E state. Substituting $p_{eg} \sim 10^{-17}$ CGSE and $\gamma \sim 10^{15}$ s^{-1}, we obtain the estimate $b \sim 10^{-5}$ provided that the laser radiation intensity is measured in W/cm^2. It was assumed that, for the optical excitation, the selection rules $\Delta m_S = 0$ were satisfied and that the excitation probabilities $T \longrightarrow T'$ ($T = X, Y, Z$; $T' = X', Y', Z'$) are the same and equal to B. Analogously, the spontaneous transitions $T' \longrightarrow T$ were assumed to occur with the same rate A, whose value for NV centers in diamond nanocrystals amounts to 7 MHz [24]. The ISC transitions $T' \longrightarrow {}^1A$ and ${}^1A \longrightarrow T'$ were taken into account in the equations for the density matrix by the rate constants $k_{T'S}^0$ and $k_{ST'}^0$, to which an optical contribution was added, which was represented by terms proportional to the intensity I_{opt}: $k_{T'S}^{\text{opt}} I_{\text{opt}}$ and $k_{ST'}^{\text{opt}} I_{\text{opt}}$. The transitions between the spin sublevels of the ground electronic state ^3A occurring under the action of the environment (spin–lattice, spin–spin, electron–phonon, etc., interactions) were taken into account with the help of the corresponding rate constants d_{ij}. For simplicity, it was assumed that $d_{XZ} = d_{YZ} = d_{ZX} = d_{ZY} = d$.

The descriptions of both the action of the MW radiation on the electron spin of the NV center and the action of the RF radiation on the nuclear spin of the NV + ^{13}C center in the density matrix equations were as detailed as necessary. In particular, the coherence induced by these radiations was taken into account. This coherence is described by the nondiagonal elements ρ_{ij}^t, where $i \neq j$ are the corresponding levels of the NV or NV + ^{13}C center coupled by the MW or RF field. In the case of the nondark OD ESR spectra (Fig. 3a) and optically detected electron spin nutations of ordinary single NV centers (Figs. 4a–4c), as well as OD ESR spectra of single NV + ^{13}C centers, the decay of the elements ρ_{YZ}^t (and ρ_{XZ}^t) was described by the rates $\Gamma_{YZ} = \Gamma_{YZ}^0 + (B_Y + B_Z)/2$, where $\Gamma_{YZ}^0 = K_{YZ}^0 + 3d/2$ is the dephasing rate in the absence of the laser radiation. The latter rate contains the term K_{YZ}^0, which has its origin in the energy fluctuations of the Y and Z states, e.g., due to mutual flipping of the electron spins of the $P1$ centers (the substitutional nitrogen atoms, $S = 1/2$) in the nanocrystal. This rate also contains the terms related to the phase interruption due to transitions from the Y and Z states to other spin states of the triplet spin of the NV center, which can be induced, e.g., by spin–lattice or spin–spin relaxation. In describing the pulsed dark experiments, all the terms depending on the optical radiation intensity were taken into account in the density matrix equations at the stage of the action of the laser pulse and were eliminated from these equations after its cessation. In all the cases, the action of the MW field on the corresponding quasi-resonance transition was considered in the rotating wave approximation. In describing the interaction with the RF field, this approximation was not used.

The equations for the elements of the density matrix were written in the matrix form by introducing the pseudospin vector R^t, composed of the elements ρ_{ij}^t: $R^t = [\rho_{X'X'}^t, \rho_{Y'Y'}^t, \rho_{Z'Z'}^t, \rho_{XX}^t, \rho_{YY}^t, \rho_{ZZ}^t, \rho_{ZY}^t, \rho_{YZ}^t, \rho_{ZX}^t, \rho_{XZ}^t, \rho_{XY}^t, \rho_{YX}^t]'$. In the case of the optically detected ESR experiments (Figs. 3a, 3b, 4, and 5), such equations have the form of an inhomogeneous matrix equation

$$dR^t/dt = MR^t + R_0, \tag{1}$$

in which the elements of both the matrix M and the vector R_0 do not depend on time and are expressed through the photophysical parameters B, A, $k_{T'S}$, $k_{ST'}$, and d_{ij}, as well through the Rabi frequency V_1 of the MW radiation (which is considered to be the same for the Z–X and Z–Y transitions) and the resonance detunings $\omega_{XZ} - \omega_1$ and $\omega_{YZ} - \omega_1$ of the MW radiation with respect to the frequencies of the Z–X and Z–Y transitions. The explicit forms of the matrix M and vector R_0 can be easily obtained if one eliminates the population of the singlet state from the density matrix equations taking into account the normalization condition $\sum \rho_{ii}^t = 1$ and passes to the basis rotating with the frequency ω_1 of the MW radiation. Upon calculation of each OD ESR spectrum, the stationary solution $R^{\text{st}} = -M^{-1}R_0$ to Eq. (1) was

sought and the fluorescence intensity spectrum $I_{fl}^{st} = A(\rho_{X'X'}^{st} + \rho_{Y'Y'}^{st} + \rho_{Z'Z'}^{st})$ was calculated in relation to the MW frequency ω_1 as this frequency was scanned through the *Z*–*X* and *Z*–*Y* resonances. The result of the fitting of the calculated and measured OD ESR spectrum of the ordinary NV center is shown by the solid line in Fig. 3a. The corresponding parameters of the model are listed in the legend of this figure. Similarly, the solid line in Fig. 3b shows the fitted OD ESR spectrum of the single NV + ^{13}C center. The parameters of the model for this center were the same as for the ordinary NV center (Fig. 3a).

To describe the nondark electron spin nutations of the single NV center under the action of the pulsed MW radiation (Fig. 4), the transient solutions $R^t = \exp(Mt)(R_{in} - R^{st}) - R^{st}$ to Eq. (1) were sought for different time intervals, where R_{in} is the corresponding initial state of the system for the given interval. Then, the transient fluorescence intensity emitted by the single center $I_{fl}^t = A(\rho_{X'X'}^t + \rho_{Y'Y'}^t + \rho_{Z'Z'}^t)$ was calculated. The nondark electron spin nutations calculated with the photophysical parameters found upon fitting of the data of Fig. 3a are shown in Figs. 4d–4f for three experimentally measured values of the power of the laser radiation $P_{opt} = I_{opt} S$. The typical value of the diameter of the focused laser beam, equal to 0.5 μm, was used to relate the experimentally measured power P_{opt} of the laser radiation with the unknown intensity I_{opt} of the laser beam focused onto the location region of the NV center. The dephasing rate of the electron spin in the ^3A state (without the optical contribution) was found to be equal to $\Gamma_{YZ}^0 = \Gamma_{XZ}^0 = 350$ kHz. For the Rabi frequency of the MW radiation, determining the frequency of the fluorescence nutations, we obtained a value of 4.5 MHz.

The dark electron spin nutations of the NV center (Fig. 5), as well as the nondark nutations (Figs. 4d–4f), were calculated on the basis of the transient solution of Eq. (1) for the corresponding time intervals. A preliminary analysis showed that both the laser pulse duration used in the experiments (1 μs) and the interval between the laser and MW pulses (0.1 μs) were insufficient for the center to attain a stationary state. Therefore, it turned out to be necessary to consider theoretically a rather long series of alternating laser and MW pulses and to average over this series the number of photons emitted by the center during the photon-counting time ($T_{count} = 0.3$ μs) for each laser pulse in the series, $n_{av} \sim \int_0^{T_{count}} I_{fl}^t dt$. The calculations showed that, if $N > 10$, where N is the number of the laser and MW pulses in the series, the number of fluorescence photons n_{av} averaged over the series virtually does not depend on N. Recall that the experimental points in Fig. 5 were obtained by averaging over a series of ~10^5 laser and MW pulses. The solid lines in Fig. 5 correspond to the calculations for three different values of the Rabi frequency of the MW radiation, which were obtained by different attenuation of some initial MW radiation. Namely, the attenuations equal to 23, 17, and 12 dB correspond to the theoretical values $2V_1 = 1.9$, 3.5, and 6.1 MHz, respectively. The power of the optical radiation used in the calculations was 10 μW. The values of the remaining parameters of the model were the same as those found upon fitting of the optically detected nondark nutations (Fig. 3).

Upon measurement of the ODENDOR spectrum (Fig. 3c), as well as of the optically detected nutations of the ^{13}C nuclear spin (Fig. 6), the MW field acts on the **1**–**3** channel of the NV + ^{13}C center and, simultaneously, the RF field acts on the **2**–**3** channel of this center. In this case, the matrix equation for the pseudovector R^t takes the form

$$dR^t/dt = [M + iV_2M_2(e^{i\omega_2 t} + e^{-i\omega_2 t})]R^t + R_0, \quad (2)$$

where V_2 and ω_2 are the Rabi frequency and the frequency of the RF field, respectively, and M_2 is a constant matrix whose elements are equal to 0 or ±1. To calculate the ODENDOR spectrum shown in Fig. 3c, the solution to Eq. (2) was written in the form of a Fourier series $R^t = \sum R^{(n)} e^{in\omega_2 t}$ and the trinomial matrix continued fraction was obtained: $(in\omega_2 + M)R^{(n)} + M_2(R^{(n+1)} + R^{(n-1)}) + R_0 = 0$ was solved for $R^{(0)}$ under the assumption that one can terminate this fraction at some term (an analysis showed that, for the parameters used, it is sufficient to take into account the terms $R^{(0)}$, $R^{(\pm 1)}$, and $R^{(\pm 2)}$). The solid line in Fig. 3c shows the fluorescence spectrum $I_{fl}^{st} = A(\rho_{X'X'}^{st} + \rho_{Y'Y'}^{st} + \rho_{Z'Z'}^{st})$ calculated in relation to the frequency of the RF field ω_2. Note that the calculated width of the ODENDOR spectrum is mainly determined by the electron spin dephasing rate K_{XY} and virtually does not depend on the ^{13}C nuclear spin dephasing rate K_{YZ}, which can be considerably smaller than K_{YZ} [7]. The calculations also showed that the splitting of the ODENDOR line is proportional to the Rabi frequency of the MW radiation V_1. This confirms the fact that this splitting results from the Autler–Townes effect, i.e., from the Stark splitting of the *Y* state due to the interaction of the *Z*–*Y* transition with the resonance MW radiation.

Finally, in order to fit the experimental data for the nuclear spin nutations of the single NV + ^{13}C center (Fig. 6), we sought the corresponding transient matrix solutions for the density matrix for the stages of action of the laser, MW, and RF pulses on the system (Fig. 6, top), respectively. As in the case of the electron spin dark nutations (Fig. 4), the amount of the fluorescence photons emitted by the center was averaged over a large series of laser pulses and this average was compared with the experiment. Since, in this case, the RF pulses act on the nuclear spin in the absence of the other fields, in Eqs. (2), one could neglect the antiresonance compo-

nent of the interaction of the spin with the RF field and, passing to the basis rotating with the frequency ω_2, transform them to the matrix equations with constant coefficients. The solid line in Fig. 6 shows the result of the fitting of the theory and experiment. In this case, the nuclear spin dephasing rate was found to be ~150 kHz, which is consistent with the experimentally estimated decay time of the nuclear spin nutations of ~2 μs [7]. It should be noted that, in diamond samples with a smaller nitrogen content, the dephasing time may achieve 100 μs [7, 25].

5. CONCLUSIONS

The theoretical modeling of the photokinetics of single NV and NV + ^{13}C centers performed on the basis of the model presented in Fig. 2, which takes into account the spin-selectivity of the ISC transitions $T' \longleftrightarrow S$, the role played by these transitions in the depletion of the singlet state at room temperature, and the particular features of the optical excitation by the Ar^+ laser, shows that the model describes well both the experimentally observed OD ESR and ODENDOR spectra of single NV and NV + ^{13}C centers and the optically detected nutations of the electron and nuclear spins of these centers caused by the action of pulsed MW and RF fields, respectively. It should be noted that, for the theoretical description of the experimental data obtained in [6, 7], it turned out to be sufficient to use common Bloch equations for the density matrix. At the same time, at low temperatures, the stochastic dynamics of the spins of *P*1 centers, which determines the dephasing rate of the electron and nuclear spins of single NV and NV + ^{13}C centers, becomes too slow. It seems that, in this case, the development of a non-Markovian theory of the spin dephasing of NV centers, similar to the theory proposed in [26], will be required for the description of these phenomena. Since, as is known [27], the spin dephasing can be suppressed by radiation, such a consideration may also be of interest in the context of the development of active methods of prolongation of the nuclear spin dephasing.

ACKNOWLEDGMENTS

This study was partially supported by INTAS (grant no. 2001-2097) and by the Belarussian Republican Foundation for Fundamental Research (grant no. F03-245).

REFERENCES

1. C. Kurtseifer, S. Mayer, P. Zarda, and H. Weinfurter, Phys. Rev. Lett. **85**, 290 (2000).
2. S. Kühn, C. Hettich, C. Schmitt, *et al.*, J. Microsc. **202**, 2 (2001).
3. J. Wrachtrup, S. Ya. Kilin, and A. P. Nizovtsev, Opt. Spectrosc. **91** (3), 429 (2001).
4. F. Jelezko, I. Popa, A. Gruber, *et al.*, Appl. Phys. Lett. **81**, 2160 (2002).
5. F. Jelezko and J. Wrachtrup, J. Phys.: Condens. Matter **16**, R1089 (2004).
6. F. Jelezko, T. Gaebal, I. Popa, *et al.*, Phys. Rev. Lett. **92**, 076 401 (2004).
7. F. Jelezko, T. Gaebal, I. Popa, *et al.*, Phys. Rev. Lett. **93**, 130 501 (2004).
8. A. P. Nizovtsev, S. Ya. Kilin, F. Jelezko, *et al.*, Opt. Spektrosk. **94** (6), 910 (2003) [Opt. Spectrosc. **94** (6), 848 (2003)].
9. E. van Oort, *Photo-dynamics of N-V Defects in Diamond, PhD Thesis* (Amsterdam Univ., Amsterdam, 1990).
10. G. Davies and N. B. Manson, *Properties and Growth of Diamond*, Ed. by G. Davies (INSPEC, London, 1994), p. 173.
11. A. Gruber, A. Dräbenstedt, C. Tietz, *et al.*, Science **276**, 2012 (1997).
12. A. Dräbenstedt, L. Fleury, C. Tietz, *et al.*, Phys. Rev. B **60**, 11 503 (1999).
13. F. Jelezko, C. Tietz, I. Popa, *et al.*, Single Molecules **2**, 255 (2001).
14. J. P. D. Martin, J. Lumin. **81**, 237 (1999).
15. E. van Oort, B. van der Kamp, R. Sitters, and M. Glasbeek, J. Lumin. **48–49**, 803 (1991).
16. A. Lenef and S. C. Rand, Phys. Rev. B **53**, 13 441 (1996).
17. S. Ya. Kilin, A. P. Nizovtsev, T. M. Maevskaya, *et al.*, J. Lumin. **86**, 201 (2000).
18. A. Beveratos, R. Brouri, J.-P. Poizat, and P. Grangier, quant-ph/0010044.
19. A. P. Nizovtsev, S. Ya. Kilin, F. Jelezko, *et al.*, Physica B **340–342**, 106 (2003).
20. A. P. Nizovtsev, S. Ya. Kilin, C. Tietz, *et al.*, Physica B **308–310**, 608 (2001).
21. J. Harrison, M. J. Sellars, and N. B. Manson, J. Lumin. **197**, 245 (2004).
22. R. H. Clarke, *Triplet State ODMR Spectroscopy* (Wiley, New York, 1982).
23. X.-F. He, N. B. Manson, and P. T. H. Fisk, Phys. Rev. B **47**, 8816 (1993).
24. A. Beveratos, R. Brouri, Th. Gacoin, *et al.*, Phys. Rev. A **64**, 061 802 (2001).
25. K. Schaumberg, E. Shabanova, J. P. F. Sellchop, and T. Anthony, Solid State Commun. **91**, 735 (1994).
26. A. P. Nizovtsev, S. Ya. Kilin, P. R. Berman, *et al.*, Phys. Rev. B **58**, 8997 (1998).
27. P. A. Apanasevich, S. Ya. Kilin, and A. P. Nizovtsev, Zh. Prikl. Spektrosk. **47**, 887 (1987).

Translated by V. Rogovoĭ